Structural Basis for the Role of Asp-120 in Metallo-β-lactamases[†,‡]

Jonathan Crisp,[§] Rebecca Conners,[§] James D. Garrity,[∥] Anne L. Carenbauer,[∥] Michael W. Crowder,[∥] and James Spencer*,[⊥]

Departments of Biochemistry and of Cellular and Molecular Medicine, University of Bristol School of Medical Sciences, University Walk, Bristol BS8 1TD, United Kingdom, and Department of Chemistry and Biochemistry, 112 Hughes Hall, Miami University, Oxford, Ohio 45056

Received April 15, 2007; Revised Manuscript Received July 9, 2007

ABSTRACT: Metallo-β-lactamases (mβls) are zinc-dependent enzymes that hydrolyze a wide range of β-lactam antibiotics. The mβl active site features an invariant Asp-120 that ligates one of the two metal ions (Zn2) and a metal-bridging water/hydroxide (Wat1). Previous studies show that substitutions at Asp-120 dramatically affect mβl activity, but no consensus exists as to its role in β-lactam turnover. Here we present crystal structures of the Asn and Cys mutants of Asp-120 of the L1 mβl from *Stenotrophomonas maltophilia*. Both mutants retain a dinuclear zinc center with Wat1 present. In the essentially inactive Cys enzyme Zn2 is displaced to a more buried position relative to that in the wild-type enzyme. In the catalytically impaired Asn enzyme the coordination of Zn2 is altered, neither it nor Wat1 is coordinated by Asn-120, and the N-terminal 19 amino acids, important to cooperative interactions between subunits in the wild-type enzyme, are disordered. Comparison with the structure of L1 complexed with the hydrolyzed oxacephem moxalactam suggests that in the Cys mutant Zn2 can no longer make stabilizing interactions with anionic nitrogen species formed in the hydrolytic reaction. The diminished activity of the Asn mutant arises from a combination of loss of intersubunit interactions and impaired proton transfer to, and reduced interaction of Zn2 with, the substrate amide nitrogen. We conclude that, while interactions of Asp-120 with active site water molecules are important to proton transfer and possibly nucleophilic attack by Wat1, its primary role is to optimally position Zn2 for catalytically important interactions with the charged amide nitrogen of substrate.

Metallo-β-lactamases (mβls) represent a growing challenge to the clinical effectiveness of β-lactams, still the most widely prescribed class of antibiotics (*1*). While bacteria have evolved a variety of methods to counter their effects (*2*), production of β-lactamases, enzymes that inactivate the antibiotic through hydrolysis of the amide bond in the four-membered β-lactam ring, is the predominant mechanism of β-lactam resistance in Gram-negative pathogens. β-Lactamases have been known since 1940 (*3*) and now number more than 500 (www.lahey.org/studies). Carbapenems, the newest and most potent generation of β-lactam agents, are now a mainstay of therapy for infection by opportunist Gram-negative organisms such as *Pseudomonas aeruginosa* and *Acinetobacter baumanii*. Colonization by such species may have serious consequences for immunocompromised individuals such as transplant, cancer chemotherapy, and HIV patients (*4*). In this context the emergence and dissemination of mβls, enzymes able to degrade almost all β-lactam classes, including carbapenems, is a particular clinical concern. None of the β-lactamase inhibitors currently in clinical use are effective against mβls (*5*, *6*), and no new antimicrobial agent with activity against pan-resistant Gram bacteria is at or near testing in clinical trials (*7*, *8*).

Mβls are prototypical members of a diverse and ancient protein superfamily with multiple hydrolytic functions (*9*). They usually contain a dinuclear active site whose two zinc ions respectively occupy a trihistidine site (Zn1), with tetrahedral geometry completed by a metal-bridging water/hydroxide moiety (Wat1), and a trigonal bipyramidal site (Zn2) with a more variable ligand set. Of the three recognized mβl subtypes (*10*), enzymes classed as B1 and B2 contain a Zn2 site with three protein ligands (Asp-120, Cys-221, and His-263), the "bridging" water/hydroxide (Wat1), and a second "apical" water molecule (Wat2), while those of subclass B3 substitute an additional histidine, His-121, for Cys-221. Asp-120 is however invariant across known mβls and almost completely conserved across the wider mβl superfamily. A number of structures of mβls and related enzymes (*11*−*21*) show the carboxylate side chain of Asp-120 to both directly ligate Zn2 and interact with the bridging water/hydroxide that is the most likely nucleophile in the hydrolytic reaction. It has consequently been inferred that Asp-120 plays an important role in the mβl-catalyzed hydrolysis of β-lactams. The absence of any covalently

[†] This work was supported by the award of a British Society for Antimicrobial Chemotherapy Vacation Studentship (J.C.), a Beit Memorial Fellowship for Medical Research (J.S.), and the U.S. National Institutes of Health (award reference GM067928).

[‡] Coordinates and structure factors have been deposited with the Protein Data Bank (www.rcsb.org; accession numbers 2QIN for the Cys mutant and 2QJS for the Asn mutant) for immediate release.

* To whom correspondence should be addressed. Phone: (44) (0) 117 331 2084. Fax: (44) (0) 117 928 7896. E-mail: Jim.Spencer@bristol.ac.uk.

[§] Department of Biochemistry, University of Bristol School of Medical Sciences.

[∥] Miami University.

[⊥] Department of Cellular and Molecular Medicine, University of Bristol School of Medical Sciences.

10.1021/bi700707u CCC: $37.00 © 2007 American Chemical Society
Published on Web 08/23/2007

Scheme 1

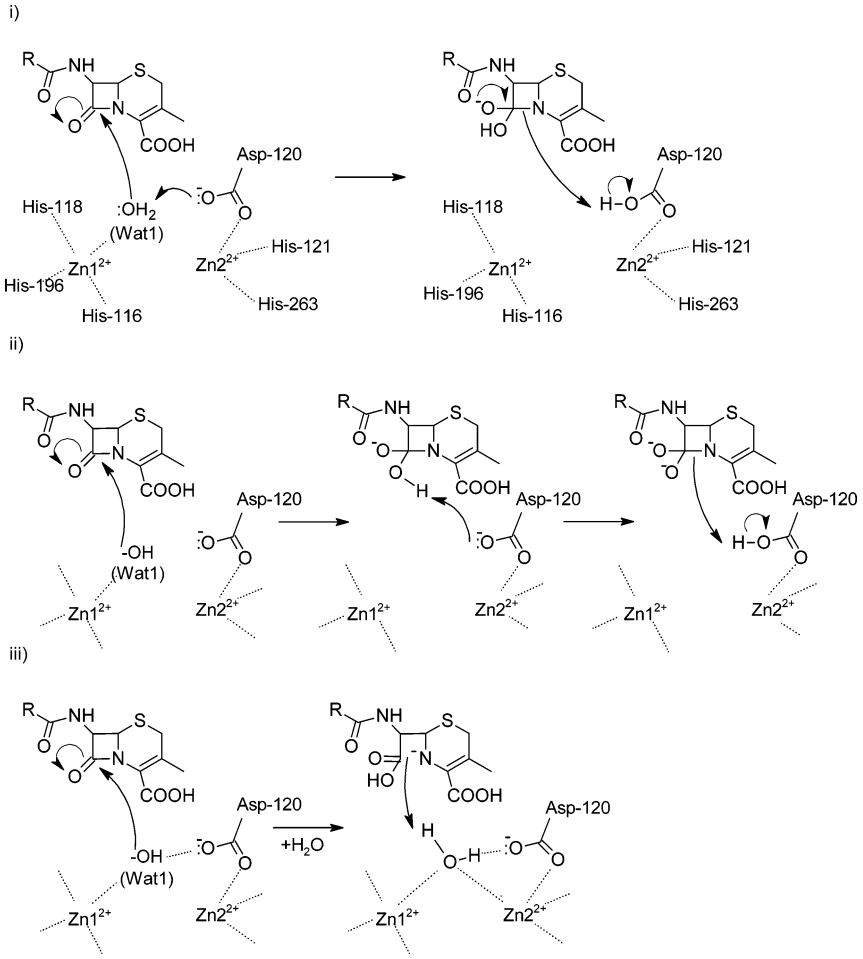

enzyme-bound intermediate rules out the possibility of Asp-120 participating in an anhydride mechanism (*22*, *23*), and a number of alternative mechanistic roles for this residue have thus been proposed (Scheme 1). These include (i) abstraction of a proton from metal-bound water (Wat1) followed by its back-donation to the amide nitrogen leaving group of the cleaved β-lactam ring (*24*), (ii) deprotonating the putative tetrahedral oxyanion intermediate formed after nucleophilic attack has occurred, thus generating a dianion whose degradation product it reprotonates (*23*), and (iii) orienting and polarizing both the metal-bound water/hydroxide (Wat1) to make the initial nucleophilic attack upon bound substrate and subsequently a second incoming water molecule that protonates the amide nitrogen and replaces Wat1 at the bridging position (*25*). It has also been suggested that Asp-120 is important in positioning Zn2 (*26*, *27*) and that this, rather than any mechanistic function, may be its primary role (*26*).

Directed mutagenesis studies confirm the conclusion that Asp-120 plays a central role in catalysis. In the subclass B1 enzyme CcrA from *Bacteroides fragilis* the Asn-, Cys-, and Ser-substituted enzymes all retain dinuclear zinc sites and are to varying degrees catalytically compromised such that activity decreases in the order Asn > Cys > Ser. Effects vary from a halving of k_{cat}/K_M (Asp-120 Asn vs imipenem (*28*)) to a 10^5-fold reduction in k_{cat} (Asp-120 Ser vs nitrocefin (*29*)). In *P. aeruginosa* IMP-1 the Asp-120 Glu and Ala mutants likewise retain the ability to bind two Zn^{2+} equivalents but show reductions in k_{cat}/K_M of up to 5 orders of magnitude (*27*), while in *Bacillus cereus* BcII a series of dinuclear Asp-120 mutants (Glu, Gln, Asn, and Ser in order of increasing effect) impaired k_{cat}/K_M by a maximum of 10^3-fold (*26*). In the subclass B3 enzyme L1 from *Stenotrophomonas maltophilia*, replacing Asp-120 with Asn or Cys generates a dinuclear enzyme where, depending on the substrate, k_{cat}/K_M is reduced by approximately 10^2-fold (Asn) or 10^3-fold (Cys). By way of contrast, the Ser mutant is a mononuclear enzyme whose activity approximates that of the Cys species, but shows impaired binding of substrate as evidenced by rapid-mixing fluorescence studies (*25*). It was concluded that, in addition to its function as a Zn^{2+} ligand, Asp-120 is involved in orienting and polarizing both the nucleophilic bridging water that attacks the β-lactam carbonyl carbon of the scissile amide bond and an incoming water molecule that serves as a proton donor to the nitrogen leaving group. Further, the retention of significant activity by the Asp-120 Asn mutant could then be explained by the possibility that the Asn amine nitrogen interacts with the metal-bridging water molecule in a fashion similar to that of the free (non-Zn^{2+}-bound) oxygen of Asp.

To investigate this hypothesis, and to establish the structural basis for the altered reactivity of Asp-120 mutants of L1, we have determined crystal structures for the two mutants Asp-120 Asn and Asp-120 Cys that retain dinuclear zinc centers. Importantly, we have obtained crystal forms of each mutant enzyme where the active site is unoccupied

by buffer ligands and at a resolution that enables Zn^{2+}-bound water molecules to be located with some confidence. The results reveal the active site of the Cys mutant to be altered from that of the wild-type enzyme primarily through a repositioning of Zn2, whereas, unexpectedly, the Asn substitution significantly affects both the coordination of Zn2 and the conformation of the extended L1 N-terminus, a region previously implicated in intersubunit interactions in the L1 tetramer (*30*). Together with existing data on the interaction of L1 with β-lactams and the kinetic effects of the two Asp-120 mutations, these results suggest that Asp-120 both acts to position Zn2 for catalytically important interactions with substrate, in particular species in which the amide nitrogen (N5) is charged, and orients Zn-bound water for protonation. We propose that these functions are of general importance to catalysis of β-lactam hydrolysis by mβls.

MATERIALS AND METHODS

Site-directed mutants of L1 were prepared and purified as described (*25*, *31*). Crystals were grown by hanging-drop vapor diffusion. L1 Asp-120 Cys was concentrated to 20 mg/mL by ultrafiltration, and drops were set up using 1 μL of protein solution mixed with 1 μL of well solution (0.1 M Tris·Cl, pH 7.5, 0.2 M $MgCl_2$, 18% PEG 4000, 5% MPD (2-methyl-2,4-pentanediol)). L1 Asp-120 Asn was concentrated to 18 mg/mL, and drops were set using 1 μL of protein solution mixed with 1 μL of well solution (0.1 M Tris·Cl, pH 8.0, 0.4 M $MgCl_2$, 21% PEG 4000). Crystallization experiments were incubated at 20 °C.

Crystals of L1 Asp-120 Cys and Asp-120 Asn were cryoprotected by transient exposure to mother liquor supplemented with 15% or 20% ethylene glycol, respectively, and frozen to 100 K. X-ray diffraction data were collected using a Quantum 4 CCD detector (Area Detector Systems Corp., Poway, CA) mounted on beamline 14.1 of the U.K. Synchrotron Radiation Source (SRS), Daresbury. Diffraction intensities were integrated, scaled, and merged using the hkl2000 suite (*32*) (HKL Research Inc., Charlottesville, VA). Structures were solved by molecular replacement with AMORE (*33*) using the unliganded L1 monomer structure (PDB ID 1SML (*31*)), with Asp-120 altered to alanine, as a search model. The Asp-120 Cys structure was refined with REFMAC 5.0 (*34*) using ARP/wARP version 5.0 (*35*) to add crystallographic water molecules. These programs were implemented under the CCP4 package (*36*). Manual rebuilding, which was largely limited to adjustment of a relatively small number of side chain positions, was carried out using COOT (*37*). However, refinement of the Asp-120 Asn mutant using this approach stalled at relatively high R_{free} values (31%), while further analysis (http://nihserver.mbi.ucla.edu/Twinning (*38*)) revealed partial merohedral twinning of this data set with a twin fraction of 0.46. Accordingly, SHELXL (*39*) was employed for the final stages of refinement. Fourfold noncrystallographic symmetry was implemented during SHELXL refinement of the Asp-120 Asn structure but was not used at any stage for L1 Asp-120 Cys.

The standard numbering scheme for mβls (*10*) has been used throughout this paper.

Table 1: Data Collection and Refinement Statistics

	Asp-120 Cys	Asp-120 Asn
beamline	SRS 14.1	SRS 14.1
wavelength (Å)	1.488	1.488
space group	$P2_1$, $a = b = 105.024$ Å, $c = 98.23$ Å	$P3_121$, $a = b = 86.382$ Å, $c = 227.363$ Å
resolution (Å)	30−1.76	50−2.25 (2.33−2.25)
R_{merge}	0.067 (0.162)	0.061 (0.517)
no. of total reflns	562 326	209 717
no. of unique reflns	98 730 (9129)	47 129 (4559)
$I/\sigma(I)$	24 (7.0)	21 (2.3)
completeness (%)	94.6 (69.9)	98.8 (97.1)
redundancy	5.7 (3.5)	4.4 (4.1)
refinement	RefMac 5	SHELXL
$R_{working}$ (%)	17.3	25.3
R_{free} (%)	21.2	28.3
rmsd bond		
length (Å)	0.006	0.012
angle (deg)	0.996	1.383
no. of protein atoms	7 940	7416
no. of water molecules	1 290	396
av B factor (Å^2)		
protein atoms	17.39	50.33
water molecules	29.52	41.92
Zn^{2+} ions	18.20	49.32

RESULTS

Crystallization and Structure Solution. Crystals of both mutant enzymes appeared within a few days of incubation. L1 Asp-120 Cys crystallized in space group $P2_1$ with cell dimensions $a = 66.14$ Å, $b = 112.85$ Å, $c = 78.35$ Å, and $\beta = 113.35°$. Volume calculations (*40*) indicated a solvent content of 47.5% with one complete L1 tetramer in the asymmetric unit. L1 Asp-120 Asn crystallized in space group $P3_121$ with cell dimensions $a = b = 86.38$ Å and $c = 227.36$ Å, suggesting a solvent content of 42.4% and one tetramer in the asymmetric unit. Reflections were observed to resolutions of 1.76 and 2.25 Å for the Asp-120 Cys and Asp-120 Asn mutants, respectively. Data collection and refinement statistics are presented in Table 1. Importantly, the excellent quality of the final electron density maps enables us to place both protein side chains and crystallographic water molecules with a high degree of confidence. Figure 1 shows the active sites of the two mutant enzymes overlaid with $F_o - F_c$ electron density maps with phases calculated using models from which the active site water molecules were omitted. Positive peaks are observed at a 3σ contour level corresponding to the positions of both bridging Wat1 and Zn2-bound apical Wat2 water molecules. Refined B factors for the bridging water molecules (four molecules in each asymmetric unit) vary between 13.34 and 19.97 Å^2 (Asp-120 Cys) and between 27.09 and 40.79 Å^2 (Asp-120 Asn), compared to average B values for main chain atoms of 16.89 and 50.68 Å^2, respectively.

L1 Asp-120 Cys. Refinement statistics for the L1 Asp-120 Cys mutant are presented in Table 1. The final refined structure contains 7940 non-hydrogen protein atoms, 8 active site Zn^{2+} ions, 1290 water molecules, 2 additional interface Zn^{2+} sites connecting His-29 of subunits B and D in tetramers of adjacent asymmetric units, and 2 Mg^{2+} ions each hexacoordinated by water molecules. The active site of the Asp-120 Cys mutant is depicted in Figure 2a. Despite the absence of any interactions with Cys-120, the bridging water

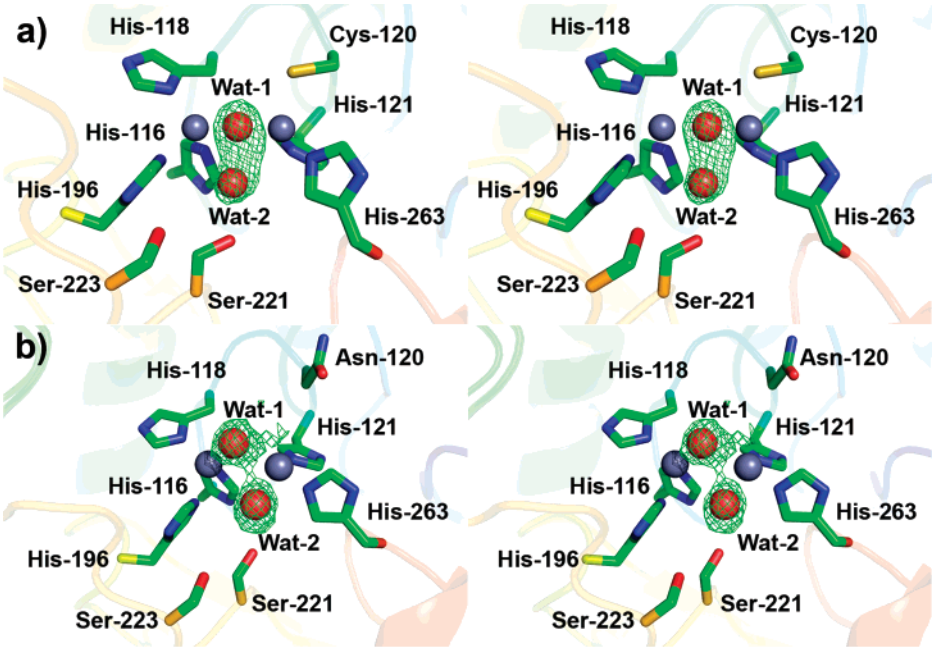

FIGURE 1: Active site stereoviews of A subunits of (a) L1 Asp-120 Cys and (b) Asp-120 Asn. The electron density shown is $F_o - F_c$, Φ_{calcd} (positive density) contoured at 3σ about active site water molecules Wat1 and Wat2. Phases were calculated using models from which both water molecules were omitted. Zinc ions are rendered as gray and water molecules as red spheres. Figures were generated using PyMol (www.pymol.org).

molecule Wat1 continues to occupy a single, well-defined position. Superposition upon the wild-type structure (*31*; Figure 2b) shows the overall structures to be very similar (overall rmsd values for Cα superposition as calculated by SSMsuperpose (*41*) vary between 0.31 Å for chain D and 0.38 Å for chain B) with little alteration in the main or side chain conformation at position 120 and Cys-120 SG adopting the same position as CG of wild-type Asp-120. However, while the Asp-120 Cys Zn1 site very closely resembles that of the wild type, mutation induces distortion about the Zn2 ion such that the $Zn^{2+}-Zn^{2+}$ distance increases by approximately 0.1 Å (range 0.08−0.15 Å for the four subunits, Table 2), and Zn2 is displaced approximately 0.7 Å (range 0.60−0.82 Å for the four subunits) from its position in the wild-type structure toward the shorter Cys side chain at position 120. The Zn2 ligands His-121 and His-263 are then displaced from their native positions and "track" Zn2 to maintain close coordination. In addition, the bridging water molecule Wat1, which in all structures of uncomplexed mβls (*21*) is located asymmetrically in the active site and lies closer to Zn1 (1.9−2.1 Å; 1.88 Å for native L1) than to Zn2 (2.1−3.1 Å; 2.06 Å for native L1), is always displaced by approximately 0.6 Å (range 0.59−0.62 Å for the four subunits) away from its position in the wild-type enzyme toward Zn2 (Wat1−Zn2 distances 1.83−2.00 Å, Table 2). In two of the four subunits (A and C) Wat1 is also significantly farther from Zn1 such that it is now asymmetrically located closer to Zn2. Furthermore, the apical water molecule Wat2 retains the position adopted in the wild-type structure, and consequently, the displacement of Zn2 effects a substantial increase in the Zn2−Wat2 distance from 2.40 to 3.07 Å (Table 2), well out of the usual range for a zinc−water ligand interaction. The conclusion that Wat2 is no longer acting as a Zn2 ligand in L1 Asp-120 Cys is supported by the elevated crystallographic *B* factors for this residue (39.3−41.0 $Å^2$), more than twice those observed for the bridging ligand Wat1 (13.34−19.97 $Å^2$; see above). This contrasts with the wild-type structure where the two water molecules have similar values (17.55 and 21.02 $Å^2$, respectively; *31*). The geometry of the Zn2 site therefore alters from trigonal bipyramidal in the wild-type enzyme to a tetrahedral arrangement in L1 Asp-120 Cys (Figure 2a), where Zn2 no longer lies in the same plane as the three axial ligands Wat1, His-121, and His-263.

L1 Asp-120 Asn. Final refinement statistics for the L1 Asp-120 Asn structure are presented in Table 1. Even though readily interpretable electron density maps were obtained after refinement with Refmac5.0, acceptable values for R_{cryst} and R_{free} resulted only after application of both twinning correction and 4-fold noncrystallographic symmetry restraints in SHELXL. The final, refined model contains 7416 non-hydrogen protein atoms and 396 water molecules. Although NCS restraints were used during refinement, they were not applied to either the active site water molecules or the Zn1−Zn2 distance. Consequently, the structure provides four alternative views of the active site (Supporting Information, Figure S1) that differ in the separation of Zn1 and Zn2 and in the disposition of water molecules in the active site.

While only weak electron density is observable for the Asn-120 side chain, inspection of $F_o - F_c$ difference maps from the early rounds of refinement, where a Zn2−Asn-120 interaction was assumed, unambiguously assigned this side chain to an orientation pointing away from Zn2 and out of the active site (Figures 3 and S1). This is the case in all four active sites in the single L1 tetramer that forms the crystallographic asymmetric unit. Contrary to earlier predictions (*25*), and despite the known ability of asparagine to act as a Zn ligand in other Zn metalloprotein structures (*42*), L1 Asn-120 does not therefore function as a Zn2 ligand in

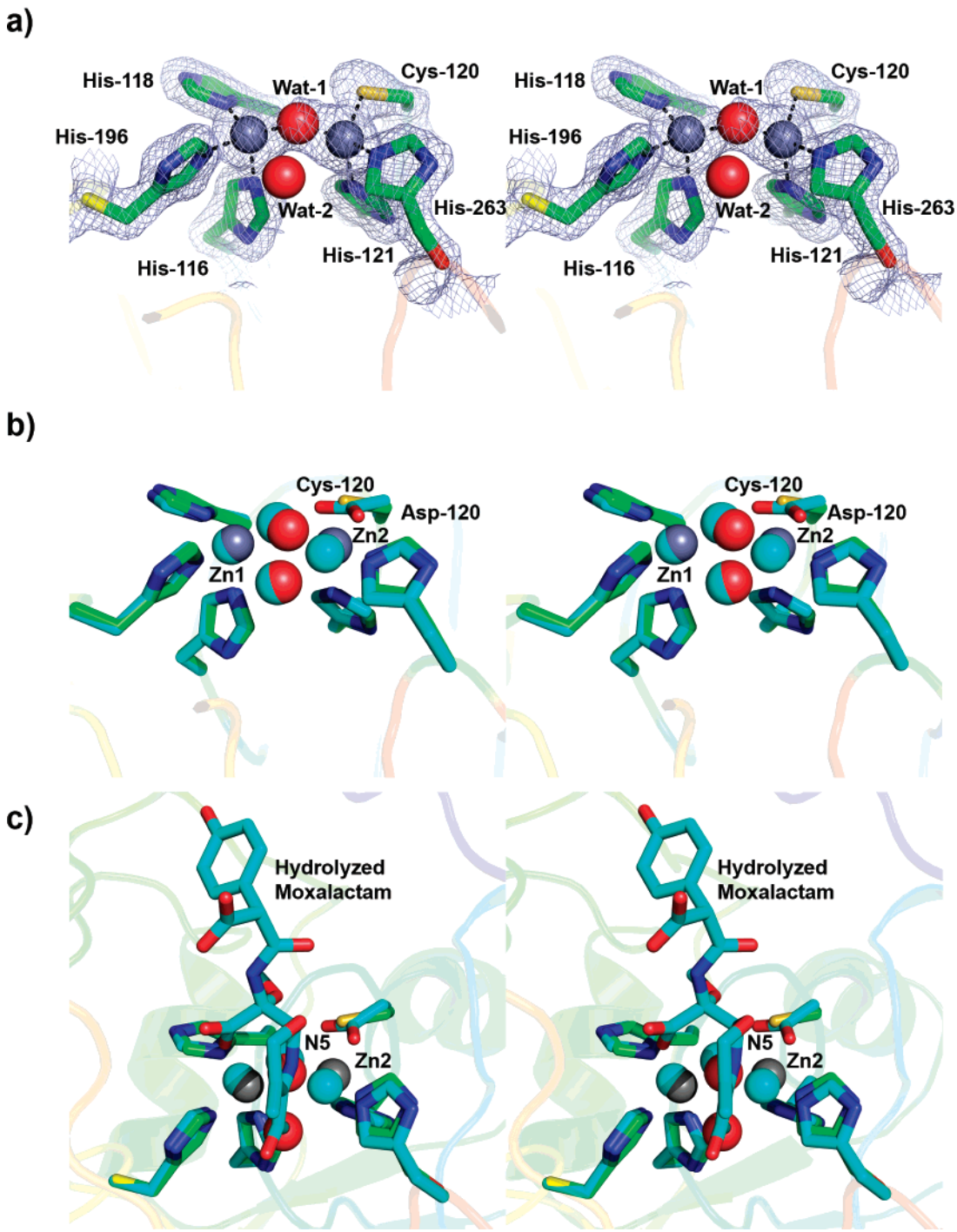

FIGURE 2: Active site stereoviews. (a) L1 Asp-120 Cys (A subunit). The electron density shown is $2F_o - F_c$, Φ_{calcd} contoured at 1.5σ. Atom colors are standard except that for carbon atoms (green). Zinc ions are rendered as gray and water molecules as red spheres. C_α carbons are rainbow-color-ramped from the N-terminal (blue) to the C-terminal (red). Zn−ligand interactions are shown as dashed lines. Note the absence of strong electron density for Wat2. (b) Superposition of the L1 Asp-120 Cys active site (A subunit; carbon atoms in green) upon that of the wild type (PDB accession 1SML (*31*); carbon atoms, zinc ions, and water molecules in cyan). (c) Superposition of the L1 Asp-120 Cys active site (A subunit; carbon atoms in green) upon that of L1 complexed with hydrolyzed moxalactam (PDB accession 2AIO (*46*); carbon atoms, zinc ions, and water molecules in cyan).

the crystallized form of the enzyme. We would however stress that our structure cannot rule out the possibility that Asn-120 is in a dynamic state where transient interactions with Zn2 remain possible.

Inspection of the L1 Asp-120 Asn structure (Figure 3a) shows that, as in the Cys mutant, the structure of the tetrahedral Zn1 site is essentially unaffected by the mutation. However, the Asp-120 Asn Zn2 site differs from that of both the wild-type and Asp-120 Cys structures. Zn2 of Asp-120 Asn is displaced from its position in the wild-type enzyme (by between 0.59 Å (subunit C) and 0.71 Å (subunit B)) out of the active site approximately along the Zn2−His-121 axis (Figure 3b). In each of the four subunits Zn2 adopts an approximately octahedral geometry that is distinct from both

Table 2: Details of Zinc Coordination in L1 Wild-Type, Mutant, and Moxalactam Complex Active Sites

atom/molecule 1	atom 2	distance in unliganded structure (*31*) (Å)	distance in L1 Asp-120 Cys, subunit A (Å)	distance in L1 Asp-120 Asn, subunit A (Å)	distance in moxalactam complex structure (*46*) (Å)
His 116 NE2	Zn1	2.03	2.14	2.08	2.20
His 118 ND1	Zn1	2.11	2.07	2.09	2.08
His 196 NE2	Zn1	2.05	2.04	2.07	2.07
Wat1	Zn1	1.88	2.05	2.00	1.99
Asp 120 OD2	Zn2	2.07			2.19
Cys 120 SG	Zn2		2.38		
Asn 120 ND	Zn2			5.27	
His 121 NE2	Zn2	2.02	2.03	2.06	2.09
His 263 NE2	Zn2	2.07	2.09	2.09	2.10
Wat1	Zn2	2.06	1.83	2.51	2.15
Wat2	Zn2	2.40	3.07	2.19	
Asp 120 OD1	Wat1	2.83			2.46
Zn1	Zn2	3.46	3.54	3.66	3.68

the trigonal bipyramidal arrangement of the wild-type enzyme and the tetrahedral geometry of L1 Asp-120 Asn (Figure S1). However, in the absence of a protein ligand at position 120, two or three coordination positions are vacant. In all four subunits Zn2 is coordinated by His-121, His-263, and the apical water molecule Wat2. In subunits A, B, and C the bridging water molecule Wat1 provides a fourth ligand, but in subunit D there is a clear discontinuity in the electron density between the two Zn^{2+} ions, and we therefore, conclude that Wat1 is most likely absent. Where Wat1 is present, it always lies closer to Zn1 (2.00 Å/1.85 Å/2.05 Å) than to Zn2 (2.51 Å/2.24 Å/2.26 Å) but is displaced from its wild-type location by between 0.24 Å (subunit B) and 0.74 Å (subunit C) to "track" the relocation of Zn2. In subunit A alone, a fourth active site water molecule, Wat4, provides an additional Zn2 ligand to complete five of the six positions in the octahedral coordination shell (Figure 3a). Thus, despite this variable ligation by water molecules, Zn2 coordination is in all cases best described by an octahedral geometry with vacant ligand positions rather than by tetrahedral or (wild-type-like) trigonal bipyramidal arrangements.

The significant intersubunit variation in Zn2 coordination suggests that the L1 Asp-120 Asn active site is less rigidly defined than its wild-type progenitor. Two additional observations provide further support for this conclusion. In wild-type L1 the $Zn^{2+}-Zn^{2+}$ distance is 3.46 Å (Table 2), a value that is consistent both with other mβls and related enzymes and with other dinuclear metallohydrolases (*21*, *43*). In the four subunits of L1 Asp-120 Asn the separation of the two metal ions varies between 3.66 Å (subunit A) and 4.06 Å (subunit D, where the bridging water Wat1 was not observed). This is in accordance with the results of molecular dynamics simulations of both uncomplexed *B. fragilis* CcrA (*44*) and a complex of *P. aeruginosa* IMP-1 with the cephalosporin cephalothin (*45*), where in both cases disruption of the Wat1 $Zn^{2+}-Zn^{2+}$ bridge leads to a significant increase in the $Zn^{2+}-Zn^{2+}$ distance. Most strikingly, although the overall fold of L1 Asp-120 Asn closely resembles that of wild-type L1 (overall C_α rmsd values vary between 0.47 and 0.59 Å), no electron density was observed for the N-terminal 19 amino acids (residues 22−40 inclusive in the standard mβl numbering scheme (*10*)), even though electrospray mass spectrometry of the protein sample prior to crystallization confirmed this region to be present after post-translational removal of the signal polypeptide.

DISCUSSION

Both the L1 Asp-120 Cys and Asp-120 Asn structures thus confirm earlier biochemical results (*25*) showing that both mutants retain dinuclear Zn^{2+} sites in which (with the sole exception of subunit D of Asp-120 Asn) the two metal ions are bridged by the probable reaction nucleophile Wat1. However, despite (i) the overall resemblance of both active site structures to that of wild-type L1, (ii) the retention of the bridging water molecule Wat1, and (iii) experimentally determined K_S values for nitrocefin binding that are close (Asp-120 Asn) or identical (Asp-120 Cys) to those obtained with the wild-type enzyme, the activities of the two mutants are significantly retarded (Asp-120 Asn) or almost entirely abolished (Asp-120 Cys). We therefore sought to better understand the effects of mutation on activity by superimposing the structures of the two mutant enzymes upon that of wild-type L1 in complex with the hydrolyzed oxacephem moxalactam (*46*; Figures 2c and 3b). The results, as we discuss below, show that the relatively small, but nonequivalent, movements of Zn2 that are occasioned by the two mutations may nevertheless have important consequences for the catalytic capabilities of the mutant enzymes.

The complex of L1 with hydrolyzed moxalactam reveals a hexacoordinate (octahedral) Zn2 ion ligated by two moxalactam functional groups, the carboxylate at C4 and the stable N5 imine nitrogen formed on loss of the 3′ leaving group. We have accordingly suggested that contact between Zn2 and the amide (imine) nitrogen N5 facilitates β-lactam hydrolysis by stabilizing accumulating negative charge during and after amide bond cleavage (Scheme 2(i); *46*). Similarly, during hydrolysis of the chromogenic substrate nitrocefin by L1 and some other mβls (*47*−*49*), a highly populated intermediate is observed with a characteristic absorbance at 665 nm that is red-shifted relative to that of either intact nitrocefin (λ_{max} 390 nm) or the product of β-lactamase-catalyzed hydrolysis (λ_{max} 482 nm). This has been ascribed to a form of hydrolyzed nitrocefin in which a deprotonated N5 nitrogen is stabilized by a combination of conjugation in the 3′-dinitrostyryl side chain and proximity to Zn2 (Scheme 2 (ii); *22*). Taken together, these observations suggest that the interaction between Zn2 and the β-lactam amide nitrogen N5 is catalytically significant.

The superposition shown in Figure 2c reveals that, in the L1 Asp-120 Cys active site, movement of Zn2 by 0.7 Å from

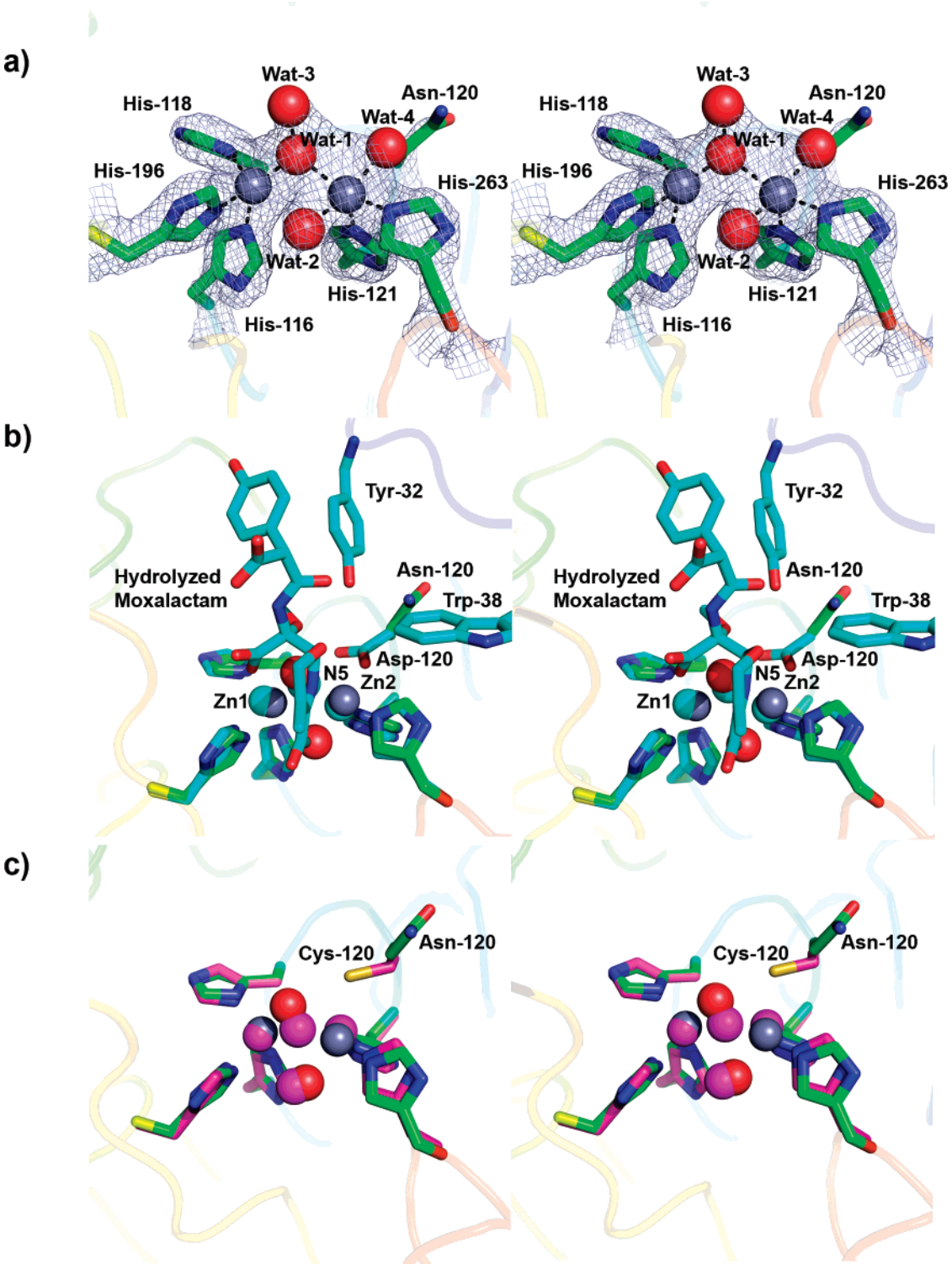

FIGURE 3: Active site stereoviews. (a) L1 Asp-120 Asn (A subunit). The electron density shown is $2F_o - F_c$, Φ_{calcd} contoured at 1.5σ. Atom colors are standard except that for carbon atoms (green). Zinc ions are rendered as gray and water molecules as red spheres. C_α carbons are rainbow-color-ramped from the N-terminal (blue) to the C-terminal (red). (b) Superposition of the L1 Asp-120 Asn active site (A subunit; carbon atoms in green) upon that of L1 complexed with hydrolyzed moxalactam (PDB accession 2AIO (*46*); carbon atoms, zinc ions, and water molecules in cyan). (c) Superposition of the L1 Asp-120 Cys active site (A subunit; carbon atoms in green) upon that of L1 Asp-120 Cys (carbon atoms, zinc ions, and water molecules in magenta).

its position in the wild-type structure toward Cys-120 is sufficient to impair formation of this interaction. In the moxalactam complex structure, Zn2 shows near-perfect octahedral coordination and is located in the same plane as the four ligands moxalactam amide nitrogen N5, Wat1, and Nϵ of His-121 and His-263. However, in the Asp-120 Cys structure Zn2 is pulled out of this plane to maintain ligation by Cys-120. Coordination of Zn2 by incoming substrate N5 at a position equivalent to that observed in the moxalactam complex will be possible only with a significant distortion away from octahedral geometry. Our conclusion is therefore that this repositioning of Zn2 significantly impairs the

Scheme 2

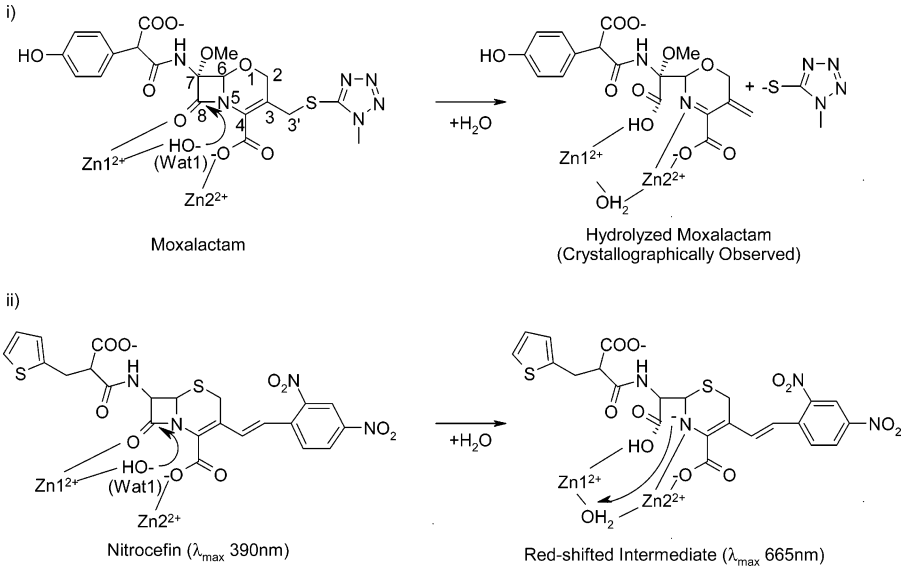

catalytic activity of L1 Asp-120 Cys by effectively preventing the stabilizing interaction of Zn2 with transition and intermediate states of bound β-lactams in which N5 is charged. This inference is supported by the absence of any observable red-shifted intermediate on nitrocefin hydrolysis by this mutant (*25*).

In contrast, L1 Asp-120 Asn does display hydrolytic activity against a range of β-lactam substrates. An explanation for the retention of significant activity is provided by comparison with both the moxalactam complex and Asp-120 Cys structures (Figure 3b,c). Although Zn2 of L1 Asp-120 Asn is displaced from its position in the wild-type enzyme and exhibits altered coordination geometry, in contrast to L1 Asp-120 Cys, the new location does not preclude interactions with bound β-lactams equivalent to those evident in the moxalactam complex. Whereas in the Asp-120 Cys mutant Zn2 is more buried as a consequence of its displacement toward Cys-120 from its position in the wild-type structure, Zn2 of Asp-120 Asn appears to be more accessible through a movement out of the active site approximately along the Zn2−His-121 axis (Figure 3b,c). Although the Zn2 coordination geometry is altered to octahedral, vacant ligand positions remain appropriately located for coordination by substrate and in particular by N5. Strong evidence that β-lactams can make appropriate N5−Zn2 interactions with L1 Asp-120 Asn is provided by formation of the red-shifted anionic nitrogen intermediate on hydrolysis of nitrocefin (*25*).

While we believe that the respective repositioning of Zn2 provides the most likely mechanism for the differing effects on activity of the two Asp-120 mutants, we cannot rule out the possibility of additional effects arising from altered interactions of Zn2 with both of the active site water molecules Wat1 and Wat2. It has previously been proposed that β-lactam hydrolysis by mβls requires the bridging ligand Wat1 to detach from Zn2 and make a nucleophilic attack on the substrate amide carbonyl (*50*) and that Wat2 (or water from bulk solvent) can then move into the vacated bridging coordination position and subsequently protonate N5 (Scheme 1 (iii); *21*, *25*, *29*). Our structures suggest that alterations in Zn2 coordination in the two mutants may be detrimental to both of these events.

Displacement of Wat1 away from its location in the wild-type structure, or loss of interaction with Asp-120 (Scheme 1 (iii)), could affect its ability to make a nucleophilic attack on the substrate carbonyl carbon that is most likely optimally positioned for addition of a Zn1-bound nucleophile. In L1 Asp-120Cys, Wat1 lies asymmetrically with respect to the two metal ions but, in two of the four subunits, closer to Zn2 rather than Zn1 as in wild-type L1. In L1 Asp-120 Asn, Wat1 moves by up to 0.74 Å from its position in the wild-type enzyme, consistent with the requirement to maintain Zn2 coordination, and is entirely absent from one of the four subunits (Figure S1). Evidence that each of these mutations exerts some effect on steps in the hydrolytic reaction preceding proton transfer to N5 is provided by their effects on the accumulation of the red-shifted (deprotonated product) intermediate formed during nitrocefin hydrolysis (Scheme 2 (ii); *25*). The absence of any detectable intermediate on nitrocefin hydrolysis by L1 Asp-120 Cys (*25*) shows that protonation of N5 is no longer rate-determining and is therefore consistent with an impaired nucleophilic attack of Wat1 upon the substrate. In the case of L1 Asp-120 Asn the nitrocefin intermediate is substantially less populated than is the case for the wild-type enzyme, while k_{cat} is reduced by more than 2 orders of magnitude, indicating that the mutation affects the rate of its formation as well as that of its decay. Both of these effects could arise from an impaired ability of the Wat1 nucleophile to attack the (C8) carbonyl carbon of the bound substrate. However, it is equally possible that disruption of the Zn2−N5 interaction serves to destabilize both the transition state for amide bond cleavage and the red-shifted intermediate such that the nucleophilic attack and amide bond cleavage (processes that in the wild-type enzyme are kinetically indistinguishable (*47*, *48*)) and proton transfer to N5 steps occur at approximately equivalent rates (Asp-120 Asn) or as a single concerted event (Asp-120 Cys). This conclusion is to some extent supported by solvent kinetic isotope effect data for nitrocefin hydrolysis, where compared to wild-type L1 ($k_H/k_D = 2.08$) a modest reduction is observed in the case of Asp-120 Cys (1.47; *25*) and a

substantial increase for Asp-120 Asn (5.36). Neither value is consistent with the inverse effect that would be expected for a change in rate-determining step from proton transfer to nucleophilic attack (*51*). We cannot however rule out the possibility that changes in the rate-determining step serve to mask the full effect of both mutations on the initial, nucleophilic attack component of the hydrolytic reaction.

The process of proton transfer from water to N5 could be adversely affected by mutation of Asp-120. In the case of L1 Asp-120 Cys, the substantial increase in the Zn2−Wat2 distance (Table 2) could influence N5 protonation by making relocation of Wat2 to the bridging position more energetically unfavorable. Similarly, proton transfer might be retarded through loss of an orienting or polarizing interaction of a proton-donating water molecule with Asp-120. In this context it may be significant that cefoxitin, a cephalosporin that, like moxalactam, possesses a good 3′ leaving group (Scheme 2 (i)) and consequently for which N5 protonation may not be required, is the substrate whose hydrolysis is least affected by the Asp-120 Cys mutation (*25*). Nevertheless, the observation that k_{cat}/K_M for cefoxitin hydrolysis is still 10^2-fold (as opposed to 10^3-fold) reduced suggests that impaired proton transfer is not the primary cause of reduced activity in the Asp-120 Cys mutant enzyme. It is also noteworthy that, as discussed above, the solvent kinetic isotope effect for nitrocefin hydrolysis by L1 Asp-120 Cys is very close to that measured for the wild-type enzyme and proton inventory measurements are consistent with a rate-determining step for hydrolysis that involves a single proton (*25*). In contrast, the dramatic increase that is observed with L1 Asp-120 Asn is suggestive of a mechanistic alteration to involve either a quantum tunneling event or transfer of multiple protons (*51*). We believe the latter to be a more reasonable explanation. In the absence of any interaction between Asn-120 and Wat1, two of the four subunits contain an additional active site water molecule (Wat3) in close proximity to Wat1 (Figures 3a and S1). We then consider it plausible that, in L1 Asp-120 Asn, protonation of the β-lactam amide nitrogen is achieved through a proton relay among several water molecules, possibly including Wat3. Importantly, no extensive network of well-defined water molecules is present in our crystal structure. As a result such a proton relay system is likely to be relatively inefficient and will lead to significantly impaired catalytic efficiency.

In wild-type L1 (and in the moxalactam complex shown in Figure 3b) portions of the N-terminus are involved in noncovalent interactions close to the active site. Notably, Tyr-32 and Trp-38 at the base of the extended N-terminus are positioned adjacent to the Zn2 site such that Trp-38 stacks over the imidazole ring of His-263 and the phenolic ring of Tyr-32 occupies a hydrophobic pocket between Trp-38 and Ile-162 (*31*). Previous work has highlighted the importance of interactions involving the extended N-terminus to the activity of L1. N-terminal truncation of L1 reduces activity (k_{cat}/K_M) by a factor of at least 20-fold, depending on the substrate (*30*). It is then conceivable that the repositioning of the Asn-120 side chain that is evident in our structure disrupts the N-terminus of L1 through steric clashes with the side chains of both Tyr-32 and Trp-38 (Figure 3b) and that loss of these interactions, and N-terminal structure, prevents intersubunit interactions in which the extreme N-terminal region is involved. Our structure thus indicates that substitution of Asp-120 by Asn, and the consequent loss of the interaction with Zn2, generates a more flexible active site than that of the wild-type enzyme and that this in turn can hinder productive intersubunit interactions that enhance stability and activity. Mass spectrometry of crystallized Asp-120 Asn, carried out in an effort to confirm the presence of the extended N-terminal region, proved inconclusive due to the high concentration of polyethylene glycol present in the crystallization experiment. However, measurements of purified Asp-120 Asn stored for an extended period of many months did indicate proteolytic cleavage taking place within the extended N-terminal region at a number of positions up to Met-42. In comparison, wild-type L1 remains intact over similar time scales both in solution and in the crystalline state (J.S. and M.W.C., unpublished observations). This increased susceptibility to proteolytic degradation provides additional evidence that the Asp-120 Asn mutation destabilizes interactions between the extended N-terminal region and the globular core of the protein. It is important however to stress that L1 Asp-120 Asn is substantially less active than the N-terminally truncated form of the enzyme (*25*, *30*), with the catalytic efficiency (k_{cat}/K_M) against both nitrocefin and imipenem reduced by an additional 10-fold.

CONCLUDING REMARKS

The two structures that we present here serve to further define the importance of Asp-120 to the activity of mβls. Our data confirm previous biochemical studies (*25*) by demonstrating that the presence of Asp at this position is not essential for formation of a dinuclear zinc site in L1. Moreover, the resolution of the structures that we present here confirms unequivocally that an intact metal center alone is sufficient to enable the proposed reaction nucleophile Wat1 to bind in a single well-defined location. Asp-120 is therefore not essential for the bridging water/hydroxide nucleophile to adopt a defined position. Our results do however define four distinct roles for Asp-120 in *S. maltophilia* L1 and/or in the wider class of mβls. First, specifically in L1, interaction of Zn2 with a strong ligand (Asp or Cys) at position 120 contributes to the overall structural integrity of the active site and makes possible interactions with the extended N-terminus that in turn contacts neighboring subunits in the L1 tetramer. Our results thus provide a partial structural explanation for the previously observed cooperativity of L1 activity (*30*). Second, the impaired activity (especially compared with that of the N-terminally truncated enzyme (*30*)) and altered isotope effect of the Asn mutant (*25*), an enzyme that is capable of making productive interactions with the amide nitrogen of the bound substrate, show that Asp-120 does play some role in proton transfer to N5. The displacement of Asn-120 that is evident in our structure then suggests that interaction of Asp120 with water (presumably relocated Wat2) in the bridging position (Wat-1) is important to this process (*25*). Third, the relocation of Wat1 that is observed in both mutant structures indicates that Asp-120 is involved in the precise positioning of the Wat1 nucleophile. Fourth, and most significantly, both mutant structures show that perturbation of the Asp-120−Zn2 interaction by mutation displaces Zn2 away from its position in the wild-type enzyme. Comparison of our structures with that of the complex of wild-type L1 with hydrolyzed moxalactam (*46*) suggests that where, as in the Asp-120 Cys mutant, displace-

ment of Zn2 is likely to prevent interaction with the amide nitrogen of bound β-lactams, the consequences for the catalytic efficiency of L1 may be profound. Our data thus suggest that Asp-120 is required to optimally position Zn2 for interaction with the amide nitrogen (moxalactam N5) of bound β-lactam as this atom accumulates negative charge during and after bond cleavage.

Recent structural studies of (inactive) Asp-120 mutants of the subclass B1 mβls also implicate Asp-120 in positioning Zn2. In IMP-1, the Asp-120 Ala mutation abolishes Zn2 binding, while the Glu substitution both disrupts Zn2 and replaces the bridging water (Wat1) with a Zn^{2+}-bridging glutamate oxygen. These authors concluded that Asp-120 both orients the Wat1 nucleophile and positions Zn2 (*27*). Very recently, a combined structural and spectroscopic investigation of the BcII enzyme suggested that the Asp-120 Ser mutation perturbs the Zn2 site and that the primary role of this residue is therefore to position Zn2 (*26*). Interestingly, the equivalent mutation in L1 abolishes Zn2 binding (*25*), highlighting the significant structural divergence between the different mβl subclasses. The importance of Asp-120 to the integrity of the Zn2 site has also been highlighted by a comparison of the structures of mβls of subclass B1, suggesting that interactions made by the Asp-120 backbone carbonyl control Zn2 affinity (*52*), and by molecular dynamic simulations showing similar interactions to be preserved in a range of active IMP-1 mutants (*53*).

The work presented here differs from that with other mutants in three aspects. First, in contrast to previous cases, the availability of a structure of a (hydrolyzed) β-lactam complex of L1 permits rationalization of the structural consequences of mutation by direct comparison of mutant structures with the active site of a mechanistically significant complex. Second, we show that while the Zn2$-\beta$-lactam interaction is disrupted in an inactive mutant (Asp-120 Cys), in an enzyme that retains some, but reduced, activity (Asp-120 Asn) abolition of the Asp-120 contact with water in the bridging position may also be important. Third, we focus on an mβl of subclass B3, where the Zn2 site is structurally distinct from those of the enzymes above (*31*) but somewhat more representative of the wider mβl enzyme superfamily (*9*) in that it possesses a His-121 Zn^{2+} ligand as part of a His-116-Xaa-His-Xaa-Asp-His-121 sequence motif and lacks Cys-221.

We have previously suggested that the Zn2$-$amide nitrogen interaction accelerates β-lactam bond fission by stabilizing accumulating negative charge on this atom and by distorting the planar geometry of the four-membered β-lactam ring portion of bound substrates (*46*). The results presented here thus provide further evidence for the importance of this interaction to β-lactam hydrolysis by mβls. Direct interaction of transiently populated anionic species with the Zn2 equivalent metal ion is a feature of the proposed catalytic mechanisms for enzymes such as glyoxalase II (*19*), tRNase Z (*18*), and AHL-lactonase (*14*, *15*), suggesting that precise positioning of this ion by the invariant Asp-120 may be a general requirement for this type of hydrolase.

ACKNOWLEDGMENT

We thank Beth Bromley for performing mass spectrometry and Alejandro Vila and the members of his research group, in particular Leticia Llarrull and Javier González, for insightful discussions and for generously sharing data prior to publication. We also acknowledge the anonymous reviewers for constructive suggestions.

SUPPORTING INFORMATION AVAILABLE

Figure S1 depicting the active sites of the four subunits of L1 Asp-120 Asn. This material is available free of charge via the Internet at http://pubs.acs.org.

REFERENCES

1. Molstad, S., Lundborg, C. S., Karlsson, A. K., and Cars, O. (2002) Antibiotic prescription rates vary markedly between 13 European countries, *Scand. J. Infect. Dis. 34*, 366−371.
2. Fisher, J. F., Meroueh, S. O., and Mobashery, S. (2005) Bacterial resistance to beta-lactam antibiotics: compelling opportunism, compelling opportunity, *Chem. Rev. 105*, 395−424.
3. Abraham, E. P., and Chain, E. (1940) An enzyme from Bacteria able to destroy penicillin, *Nature 146*, 837.
4. Quinn, J. P. (1998) Clinical problems posed by multiresistant nonfermenting gram-negative pathogens, *Clin. Infect. Dis. 27*, Suppl. 1, S117−124.
5. Miller, L. A., Ratnam, K., and Payne, D. J. (2001) Beta-lactamase-inhibitor combinations in the 21st century: current agents and new developments, *Curr. Opin. Pharmacol. 1*, 451−458.
6. Walsh, T. R., Toleman, M. A., Poirel, L., and Nordmann, P. (2005) Metallo-beta-lactamases: the quiet before the storm?, *Clin. Microbiol. Rev. 18*, 306−325.
7. Livermore, D. M. (2004) The need for new antibiotics, *Clin. Microbiol. Infect. 10*, Suppl. 4, 1−9.
8. Livermore, D. M. (2005) Minimising antibiotic resistance, *Lancet Infect. Dis. 5*, 450−459.
9. Daiyasu, H., Osaka, K., Ishino, Y., and Toh, H. (2001) Expansion of the zinc metallo-hydrolase family of the beta-lactamase fold, *FEBS Lett. 503*, 1−6.
10. Galleni, M., Lamotte-Brasseur, J., Rossolini, G. M., Spencer, J., Dideberg, O., and Frere, J. M. (2001) Standard numbering scheme for class B beta-lactamases, *Antimicrob. Agents Chemother. 45*, 660−663.
11. Garau, G., Lemaire, D., Vernet, T., Dideberg, O., and Di Guilmi, A. M. (2005) Crystal structure of phosphorylcholine esterase domain of the virulence factor choline-binding protein e from streptococcus pneumoniae: new structural features among the metallo-beta-lactamase superfamily, *J. Biol. Chem. 280*, 28591−28600.
12. Mandel, C. R., Kaneko, S., Zhang, H., Gebauer, D., Vethantham, V., Manley, J. L., and Tong, L. (2006) Polyadenylation factor CPSF-73 is the pre-mRNA 3′-end-processing endonuclease, *Nature 444*, 953−956.
13. Hagelueken, G., Adams, T. M., Wiehlmann, L., Widow, U., Kolmar, H., Tummler, B., Heinz, D. W., and Schubert, W. D. (2006) The crystal structure of SdsA1, an alkylsulfatase from Pseudomonas aeruginosa, defines a third class of sulfatases, *Proc. Natl. Acad. Sci. U.S.A. 103*, 7631−7636.
14. Kim, M. H., Choi, W. C., Kang, H. O., Lee, J. S., Kang, B. S., Kim, K. J., Derewenda, Z. S., Oh, T. K., Lee, C. H., and Lee, J. K. (2005) The molecular structure and catalytic mechanism of a quorum-quenching N-acyl-L-homoserine lactone hydrolase, *Proc. Natl. Acad. Sci. U.S.A. 102*, 17606−17611.
15. Liu, D., Lepore, B. W., Petsko, G. A., Thomas, P. W., Stone, E. M., Fast, W., and Ringe, D. (2005) Three-dimensional structure of the quorum-quenching N-acyl homoserine lactone hydrolase from Bacillus thuringiensis, *Proc. Natl. Acad. Sci. U.S.A. 102*, 11882−11887.
16. Kostelecky, B., Pohl, E., Vogel, A., Schilling, O., and Meyer-Klaucke, W. (2006) The crystal structure of the zinc phosphodiesterase from Escherichia coli provides insight into function and cooperativity of tRNase Z-family proteins, *J. Bacteriol. 188*, 1607−1614.
17. Ishii, R., Minagawa, A., Takaku, H., Takagi, M., Nashimoto, M., and Yokoyama, S. (2005) Crystal structure of the tRNA 3′ processing endoribonuclease tRNase Z from Thermotoga maritima, *J. Biol. Chem. 280*, 14138−14144.

18. de la Sierra-Gallay, I. L., Pellegrini, O., and Condon, C. (2005) Structural basis for substrate binding, cleavage and allostery in the tRNA maturase RNase Z, *Nature 433*, 657−661.
19. Cameron, A. D., Ridderstrom, M., Olin, B., and Mannervik, B. (1999) Crystal structure of human glyoxalase II and its complex with a glutathione thiolester substrate analogue, *Struct. Folding Des. 7*, 1067−1078.
20. Frazao, C., Silva, G., Gomes, C. M., Matias, P., Coelho, R., Sieker, L., Macedo, S., Liu, M. Y., Oliveira, S., Teixeira, M., Xavier, A. V., Rodrigues-Pousada, C., Carrondo, M. A., and Le Gall, J. (2000) Structure of a dioxygen reduction enzyme from Desulfovibrio gigas, *Nat. Struct. Biol. 7*, 1041−1045.
21. Crowder, M. W., Spencer, J., and Vila, A. J. (2006) Metallo-beta-lactamases: novel weaponry for antibiotic resistance in bacteria, *Acc. Chem. Res. 39*, 721−728.
22. Wang, Z., Fast, W., and Benkovic, S. J. (1999) On the mechanism of the metallo-beta-lactamase from Bacteroides fragilis, *Biochemistry 38*, 10013−10023.
23. Bounaga, S., Laws, A. P., Galleni, M., and Page, M. I. (1998) The mechanism of catalysis and the inhibition of the Bacillus cereus zinc-dependent beta-lactamase, *Biochem. J 331*, 703−711.
24. Carfi, A., Pares, S., Duee, E., Galleni, M., Duez, C., Frere, J. M., and Dideberg, O. (1995) The 3-D structure of a zinc metallo-beta-lactamase from Bacillus cereus reveals a new type of protein fold, *EMBO J. 14*, 4914−4921.
25. Garrity, J. D., Carenbauer, A. L., Herron, L. R., and Crowder, M. W. (2004) Metal binding Asp-120 in metallo-beta-lactamase L1 from Stenotrophomonas maltophilia plays a crucial role in catalysis, *J. Biol. Chem. 279*, 920−927.
26. Llarrull, L. I., Fabiane, S. M., Kowalski, J. M., Bennett, B., Sutton, B. J., and Vila, A. J. (2007) Asp120 locates Zn2 for optimal metallo-Beta-lactamase activity, *J. Biol. Chem. 282*, 18276−18285.
27. Yamaguchi, Y., Kuroki, T., Yasuzawa, H., Higashi, T., Jin, W., Kawanami, A., Yamagata, Y., Arakawa, Y., Goto, M., and Kurosaki, H. (2005) Probing the Role of Asp-120(81) of Metallo-{beta}-lactamase (IMP-1) by Site-directed Mutagenesis, Kinetic Studies, and X-ray Crystallography, *J. Biol. Chem. 280*, 20824−20832.
28. Yang, Y., Keeney, D., Tang, X., Canfield, N., and Rasmussen, B. A. (1999) Kinetic properties and metal content of the metallo-beta-lactamase CcrA harboring selective amino acid substitutions, *J. Biol. Chem. 274*, 15706−15711.
29. Yanchak, M. P., Taylor, R. A., and Crowder, M. W. (2000) Mutational analysis of metallo-beta-lactamase CcrA from Bacteroides fragilis, *Biochemistry 39*, 11330−11339.
30. Simm, A. M., Higgins, C. S., Carenbauer, A. L., Crowder, M. W., Bateson, J. H., Bennett, P. M., Clarke, A. R., Halford, S. E., and Walsh, T. R. (2002) Characterization of monomeric L1 metallo-beta -lactamase and the role of the N-terminal extension in negative cooperativity and antibiotic hydrolysis, *J. Biol. Chem. 277*, 24744−24752.
31. Ullah, J. H., Walsh, T. R., Taylor, I. A., Emery, D. C., Verma, C. S., Gamblin, S. J., and Spencer, J. (1998) The crystal structure of the L1 metallo-beta-lactamase from Stenotrophomonas maltophilia at 1.7 A resolution, *J. Mol. Biol. 284*, 125−136.
32. Otwinowski, Z., and Minor, W. (1997) Processing of X-ray Diffraction Data Collected in Oscillation Mode, *Methods Enzymol. 276*, 307−326.
33. Navaza, J. (2001) Implementation of molecular replacement in AMoRe, *Acta Crystallogr., D: Biol. Crystallogr. 57*, 1367−1372.
34. Murshudov, G. N., Vagin, A. A., and Dodson, E. J. (1997) Refinement of Macromolecular Structures by the Maximum-Likelihood Method, *Acta Crystallogr., D: Biol. Crystallogr. 53*, 240−255.
35. Lamzin, V. S., and Wilson, K. S. (1997) Automated refinement for protein crystallography, *Methods Enzymol. 277*, 269−305.
36. Collaborative Computational Project, N. (1994) The CCP4 Suite: Programs for Protein Crystallography, *Acta Crystallogr., D: Biol. Crystallogr. 50*, 760−763.
37. Emsley, P., and Cowtan, K. (2004) Coot: model-building tools for molecular graphics, *Acta Crystallogr., D: Biol. Crystallogr. 60*, 2126−2132.
38. Yeates, T. O. (1997) Detecting and overcoming crystal twinning, *Methods Enzymol. 276*, 344−358.
39. Sheldrick, G. M., and Schneider, T. S. (1997) SHELXL:high resolution refinement, *Methods Enzymol. 277*, 319−343.
40. Matthews, B. W. (1968) Solvent content of protein crystals, *J. Mol. Biol. 33*, 491−497.
41. Krissinel, E., and Henrick, K. (2004) Secondary-structure matching (SSM), a new tool for fast protein structure alignment in three dimensions, *Acta Crystallogr., D: Biol. Crystallogr. 60*, 2256−2268.
42. Odintsov, S. G., Sabala, I., Marcyjaniak, M., and Bochtler, M. (2004) Latent LytM at 1.3A resolution, *J. Mol. Biol. 335*, 775−785.
43. Auld, D. S. (2001) Zinc coordination sphere in biochemical zinc sites, *Biometals 14*, 271−313.
44. Suarez, D., Brothers, E. N., and Merz, K. M., Jr. (2002) Insights into the structure and dynamics of the dinuclear zinc beta-lactamase site from Bacteroides fragilis, *Biochemistry 41*, 6615−6630.
45. Oelschlaeger, P., Schmid, R. D., and Pleiss, J. (2003) Insight into the mechanism of the IMP-1 metallo-beta-lactamase by molecular dynamics simulations, *Protein Eng. 16*, 341−350.
46. Spencer, J., Read, J., Sessions, R. B., Howell, S., Blackburn, G. M., and Gamblin, S. J. (2005) Antibiotic recognition by binuclear metallo-beta-lactamases revealed by X-ray crystallography, *J. Am. Chem. Soc. 127*, 14439−14444.
47. Spencer, J., Clarke, A. R., and Walsh, T. R. (2001) Novel mechanism of hydrolysis of therapeutic beta-lactams by Stenotrophomonas maltophilia L1 metallo-beta-lactamase, *J. Biol. Chem. 276*, 33638−33644.
48. McManus-Munoz, S., and Crowder, M. W. (1999) Kinetic mechanism of metallo-beta-lactamase L1 from Stenotrophomonas maltophilia, *Biochemistry 38*, 1547−1553.
49. Wang, Z., Fast, W., and Benkovic, S. J. (1998) Direct observation of an enzyme-bound intermediate in the catalytic cycle of the metallo-β-lactamase from *Bacteroides. fragilis, J. Am. Chem. Soc. 120*, 10788−10789.
50. Suarez, D., Diaz, N., and Merz, K. M., Jr. (2002) Molecular dynamics simulations of the dinuclear zinc-beta-lactamase from Bacteroides fragilis complexed with imipenem, *J. Comput. Chem. 23*, 1587−1600.
51. Schowen, K. B., and Schowen, R. L. (1982) Solvent isotope effects in enzyme systems, *Methods Enzymol. 87*, 551−606.
52. Murphy, T. A., Catto, L. E., Halford, S. E., Hadfield, A. T., Minor, W., Walsh, T. R., and Spencer, J. (2006) Crystal structure of Pseudomonas aeruginosa SPM-1 provides insights into variable zinc affinity of metallo-beta-lactamases, *J. Mol. Biol. 357*, 890−903.
53. Oelschlaeger, P., and Pleiss, J. (2007) Hydroxyl groups in the (beta)beta sandwich of metallo-beta-lactamases favor enzyme activity: Tyr218 and Ser262 pull down the lid, *J. Mol. Biol. 366*, 316−329.

BI700707U